Characterization of wood using mechanical waves

Journée Contrôle et Evaluation Non Destructive du bois

Luis ESPINOSA

Université de Technologie de Tarbes

Institut Clément Ader (ICA) – UMR CNRS 5312

Contents

I. Relationship between damping of mechanical waves and physico-mechanical properties of wood

II. Modelling wave propagation using the transmitting sensors' responses

(I) Relationship between damping of mechanical waves and physico-mechanical properties of wood

Context

- Wood material is complex to **characterize** due to its biological origin
- In the context of **NDT&E**, It is necessary to study the relationships between the **mechanical and physical characteristics of wood**, and the corresponding **acoustic properties**

Anisotropic

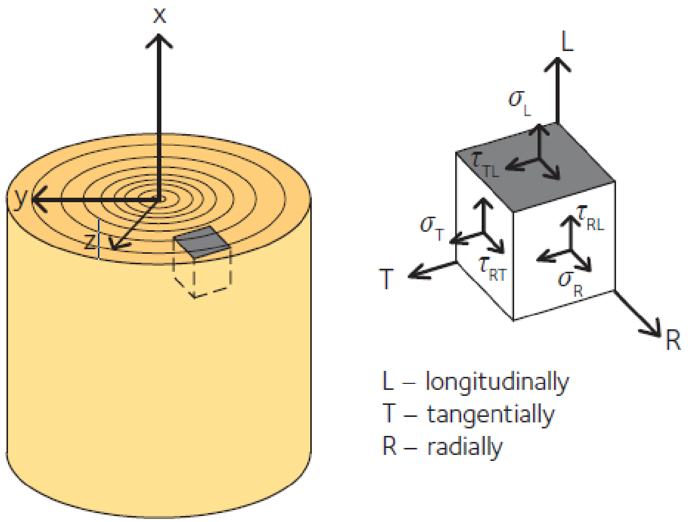

Definition of normal- (σ) and shear- (τ) stresses in different directions in wood, Design of timber structures – Volume 1 (2022)

Heterogeneous

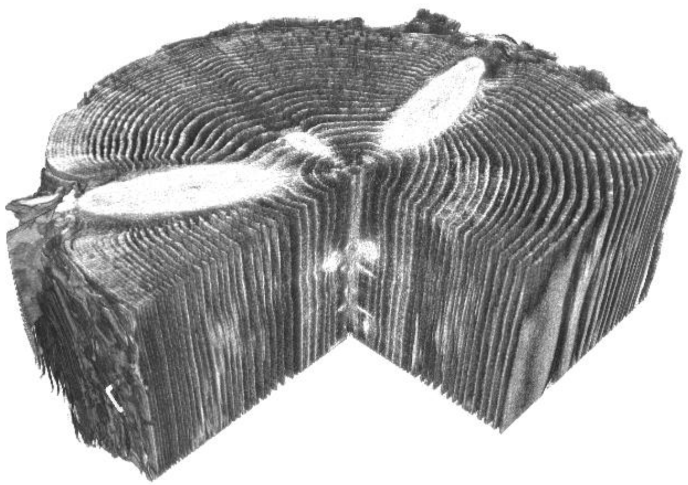

X-ray CT reconstruction of 3D density distribution in sawn wood and timber laminates, Sanabria (2012)

Hygroscopic

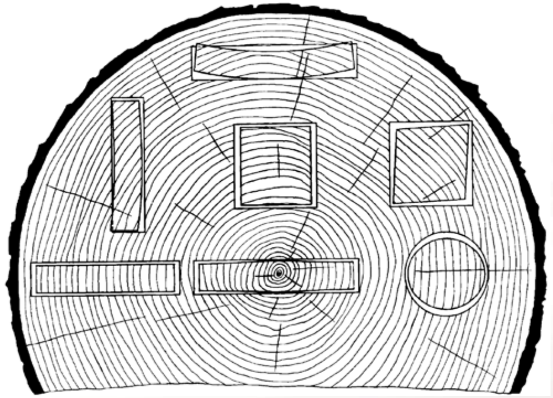

Characteristic shrinkage and distortion of flat, square, and round pieces as affected by direction of growth rings, Wood handbook (2010)

Objectif

*Evaluate the effect of the variation of physical-mechanical properties of wood associated with structural deterioration, such as the modulus of elasticity (**MOE**), and **density**, on the **attenuation** of acoustic waves propagating in wood.*

Compression and bending free-vibration tests (BING)

+

Ultrasonic testing

=

MOE and Attenuation coefficient

Materials

- A batch of 58 tropical wood specimens was taken from CIRAD’s wood collection
- Broad range of densities from 205 to 1287 kg/m3
- All specimens were stabilized in a climate-controlled room with 65% relative humidity and a temperature of 20°C and with theoretical moisture content at equilibrium of 12%

236 mm

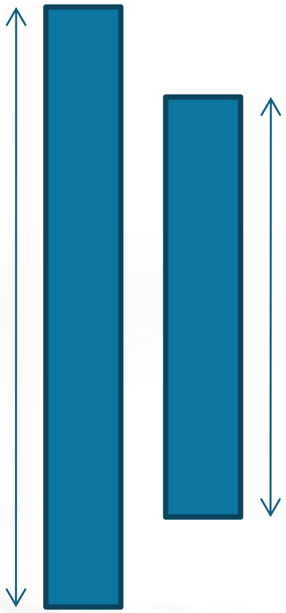

150 mm

Two different lengths for each specimen

Acoustic characterization: Bing

- For acoustic tests, BING® device was used, relying on a free-vibration analysis
- Outputs: MOE (bending and compression), loss tangent (tan δ)

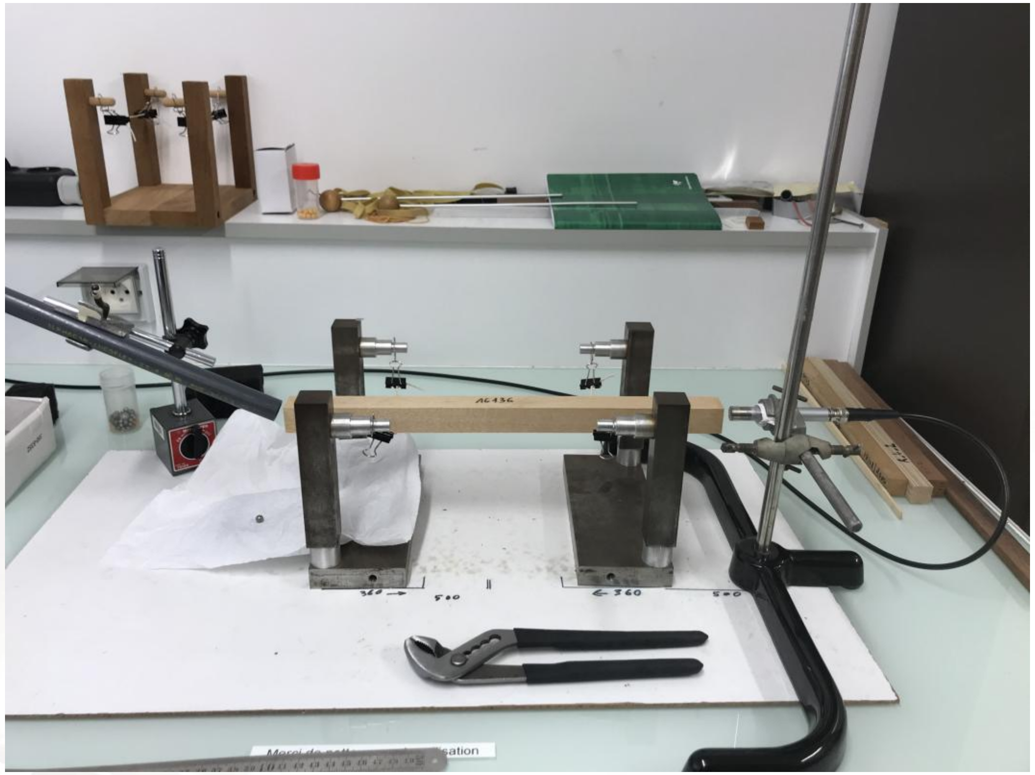

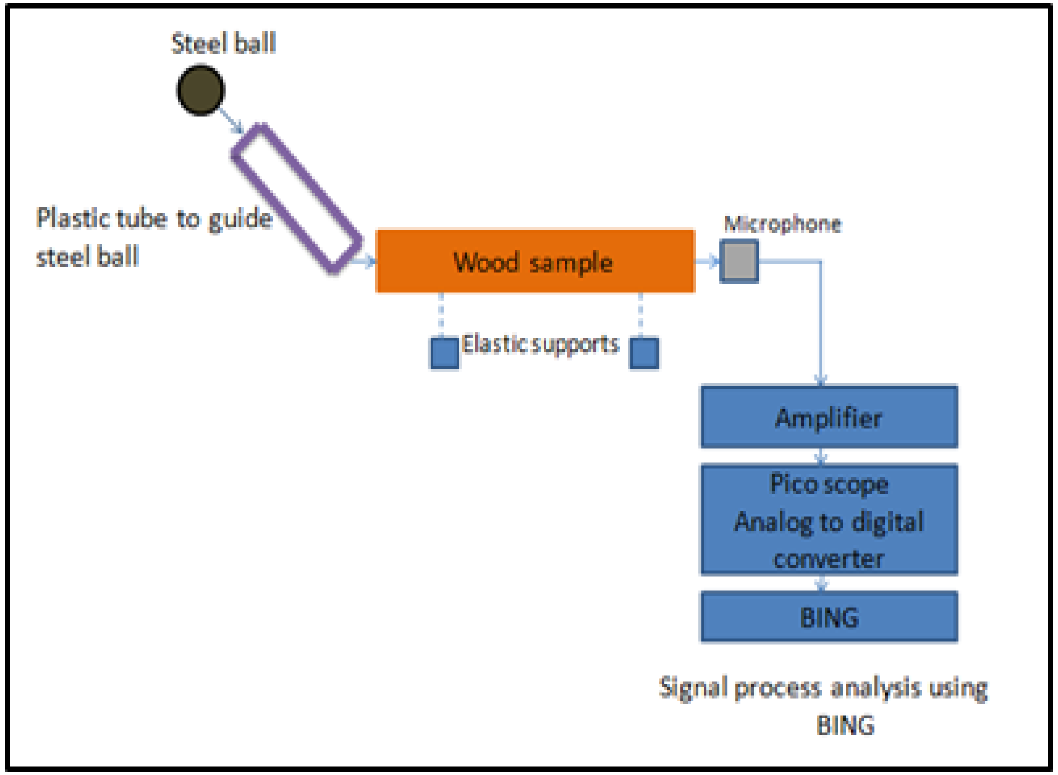

Ultrasound characterization

- For ultrasonic tests, a through-transmission configuration was used with sensors at a resonant frequency of 500 kHz
- Outputs: MOE, tan δ, attenuation coefficient α

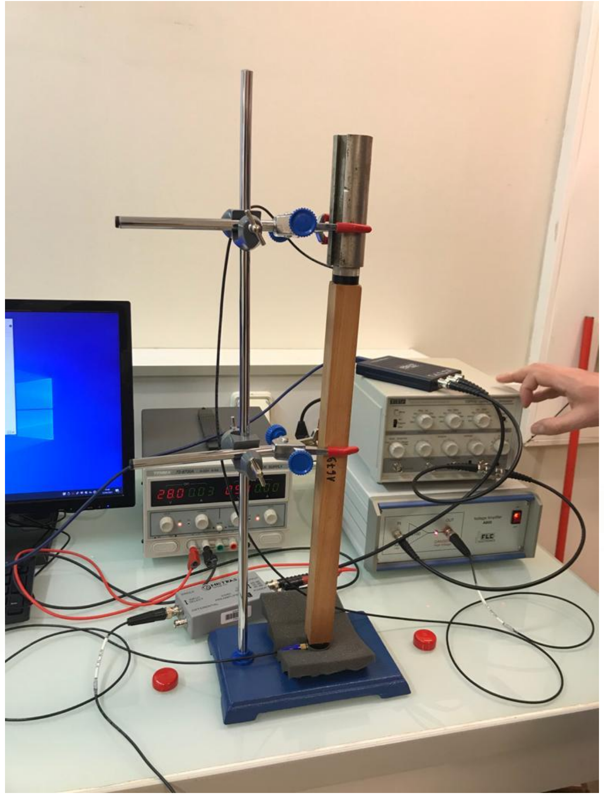

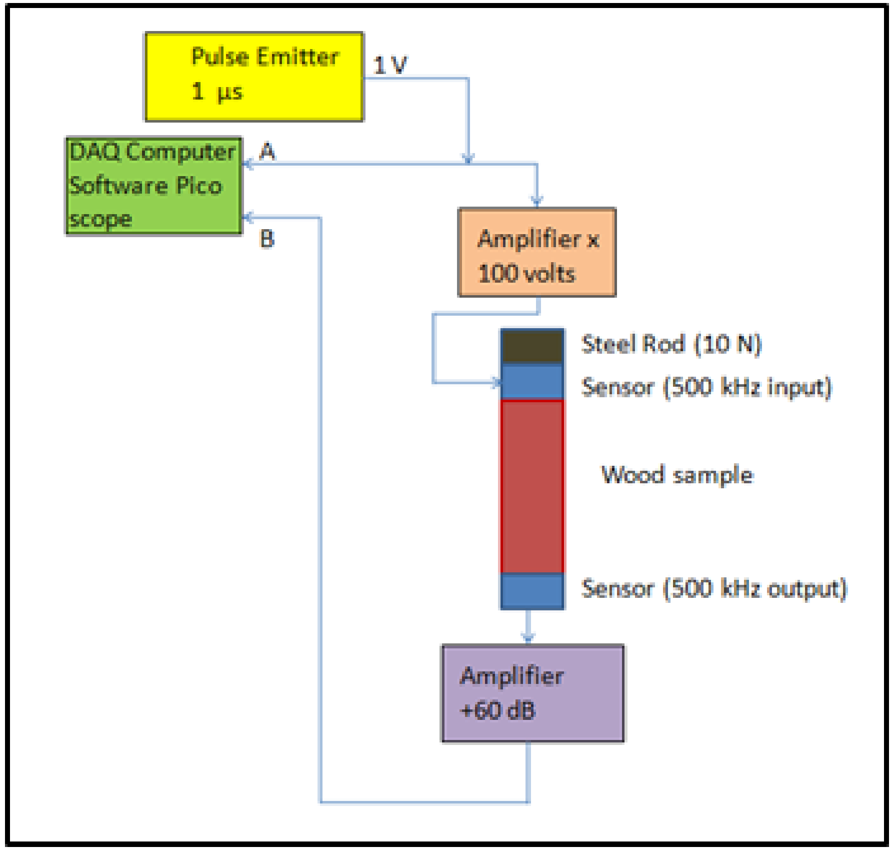

Results

Comparison between MOE from acoustic measurements for bending and compression

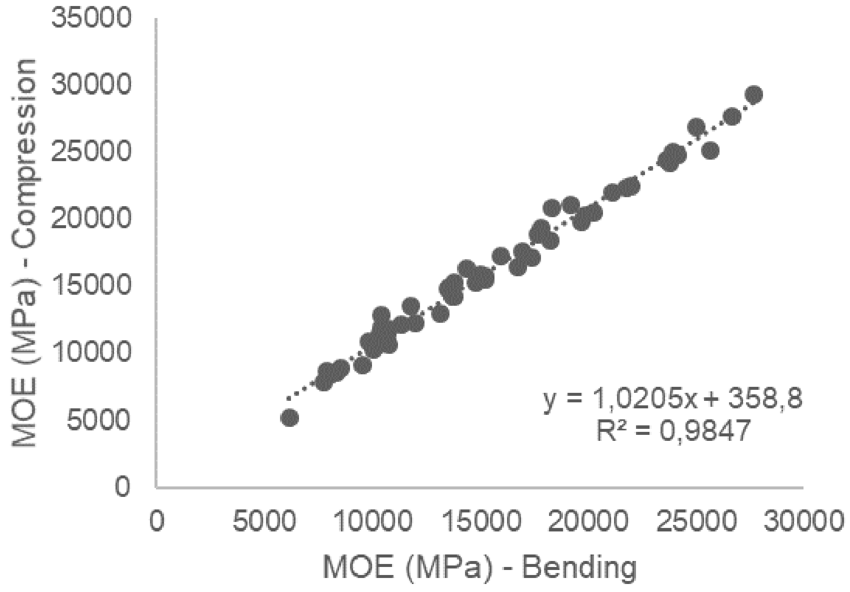

Comparison between MOE from ultrasonic and acoustic (bending) measurements

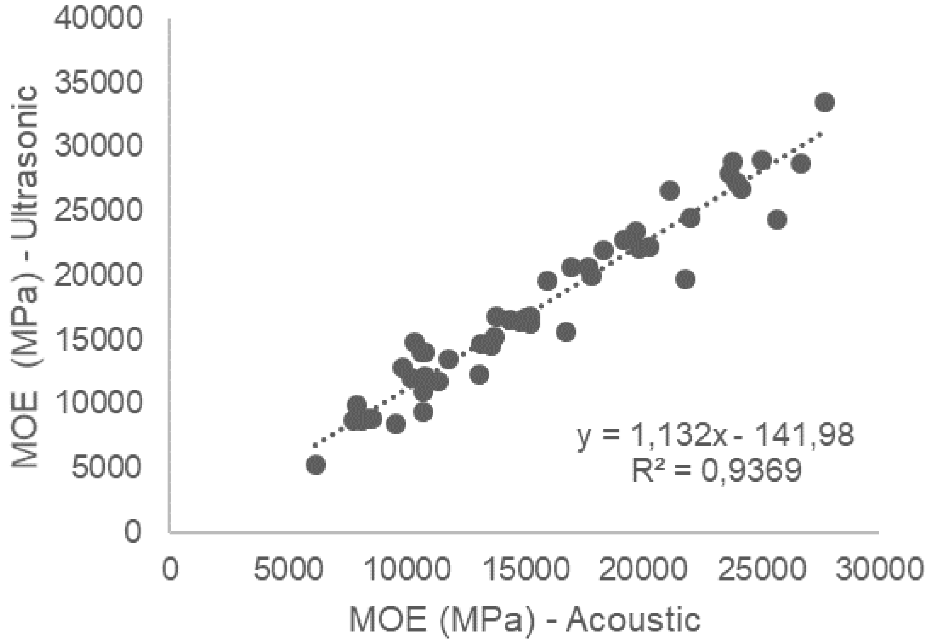

- Good agreement between the values obtained in compression and bending for the acoustic tests
- Also good agreement from the ultrasonic and acoustic (bending) tests

Results

Comparison tan δ acoustic
Bending and compression

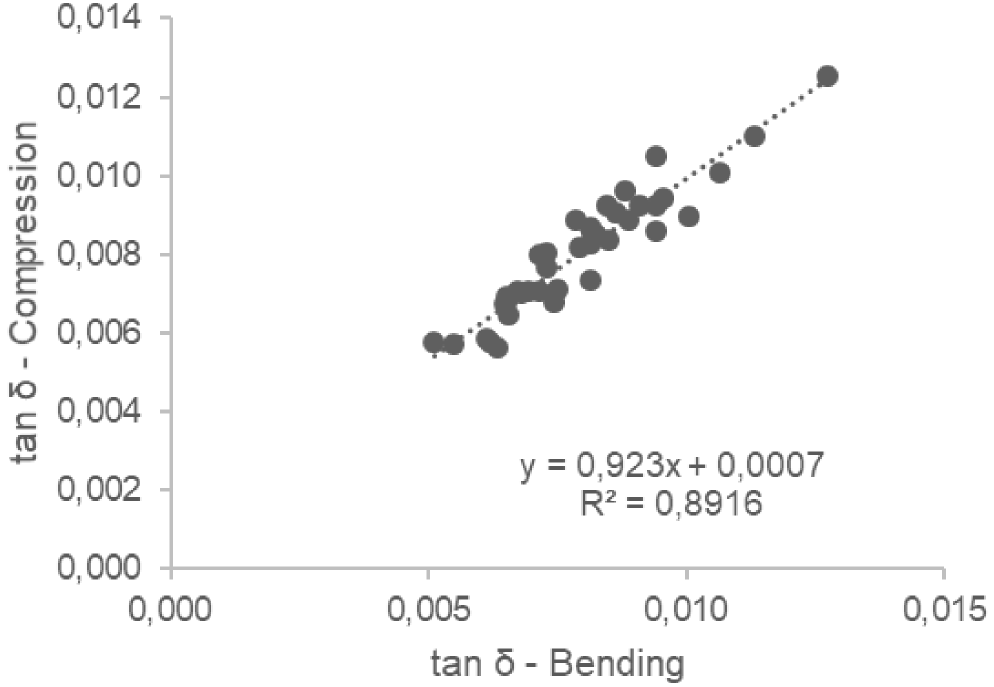

Comparison tan δ acoustic and ultrasonic

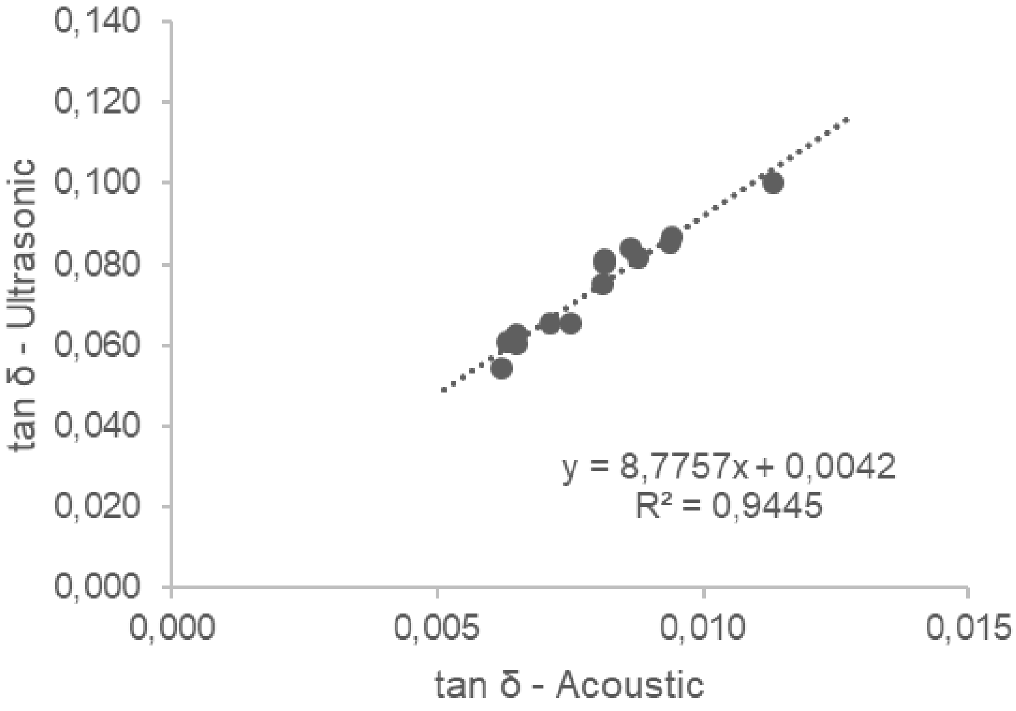

- Good agreement between the values obtained in compression and bending for the acoustic tests
- In the case of ultrasonic tests, tan δ values were larger compared to the acoustic ones

Results

Comparison MOE ultrasonic and density

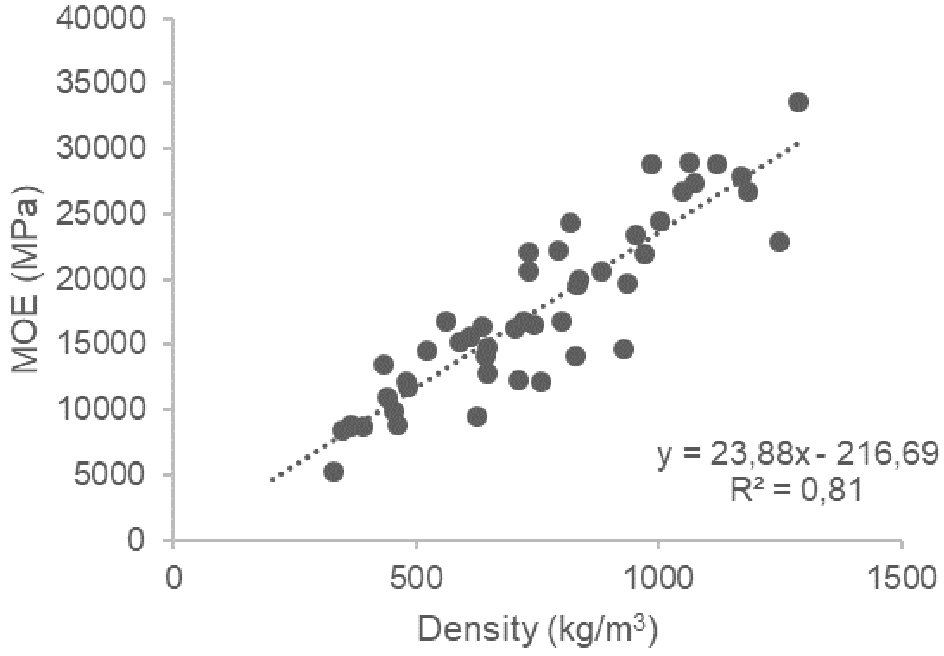

Comparison attenuation coefficient α and density

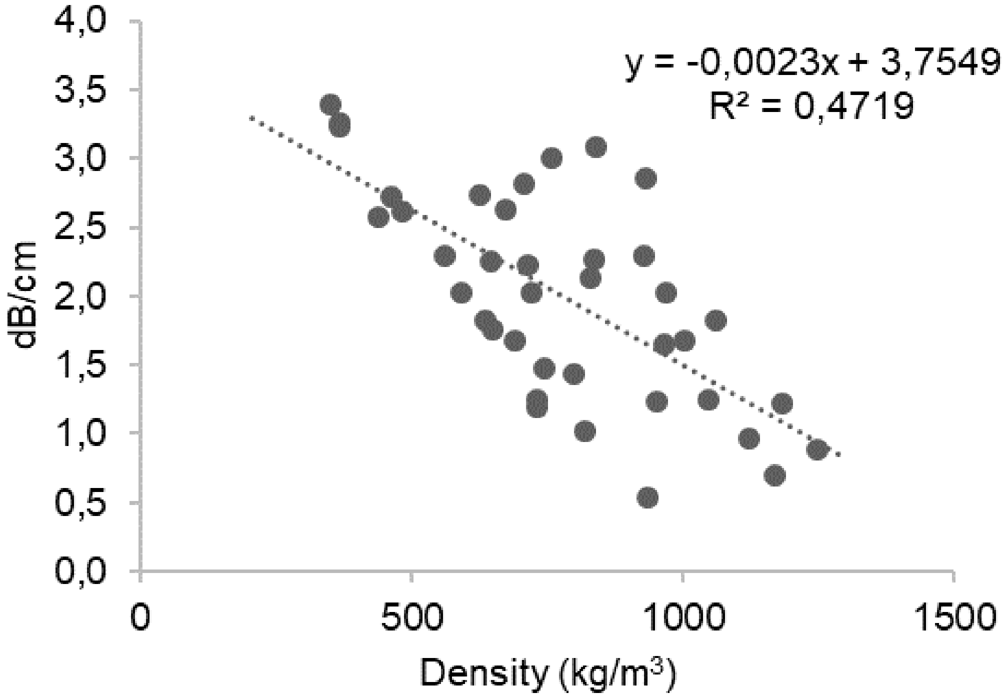

- MOE values were larger for species with higher density
- For the attenuation coefficient α the relationship was the opposite with decreasing values as the density of the sample increased

Conclusions

- The viscoelastic behavior of wood was studied through a set of experiments using acoustic and ultrasonic methods

- Good agreement was observed for the MOE and tan δ obtained either by comparing compression and bending in the acoustic case, or by comparing ultrasonic and acoustic measurements

- Density is a key parameter affecting MOE and attenuation

- Numerical modeling techniques could be a valuable tool to study the effect of the wood physical and mechanical characteristics in the propagation of elastic waves

(II) Modelling wave propagation using the transmitting sensors' responses

Context

Ultrasonic chain of measurement

Electrical impulsion $s(t)$ → Sensor + amplifier + coupling $h_t(t)$ → Sample $h_m(t)$ → Sensor + amplifier + coupling $h_t(t)$ → Output signal $y(t)$

$$y(t) = ((h_t^* * s) * h_m)\,(t)$$

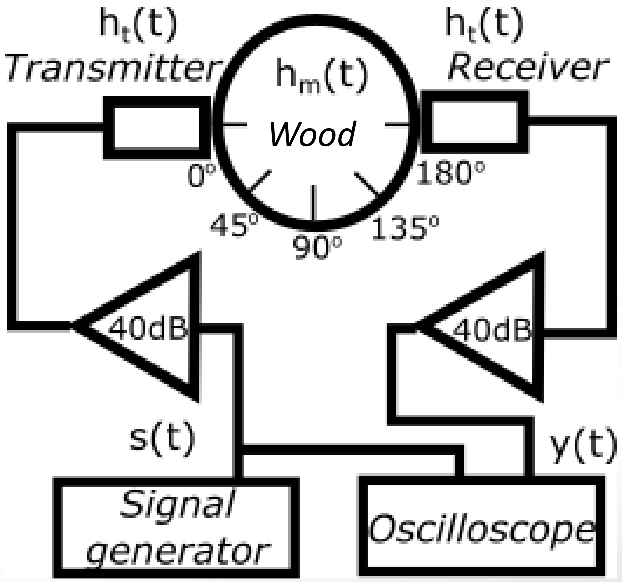

How to include the sensor transfer function on the numerical modelling of mechanical waves propagation to improve the accuracy?

h_t^*: auto-convolution of the transducers impulse response $h_t(t)$, including the response of the amplifier, and considering the transmitter and receiver transducers responses with coupling to be identical[1]

[1] *Philippe Lasaygues, Andrés Arciniegas, Luis Espinosa, Flavio Prieto, Lasaygues Philippe. Accuracy of coded excitation methods for measuring the time of flight: Application to ultrasonic characterization of wood samples*

Context

Modelling of the sensors:

Transmitting sensor's response:

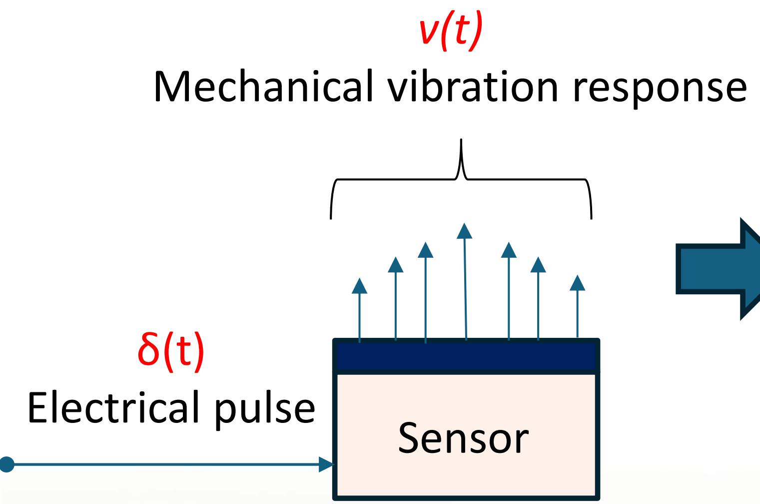

Normal velocity response on contact surface for µ80 sensor[1,3]

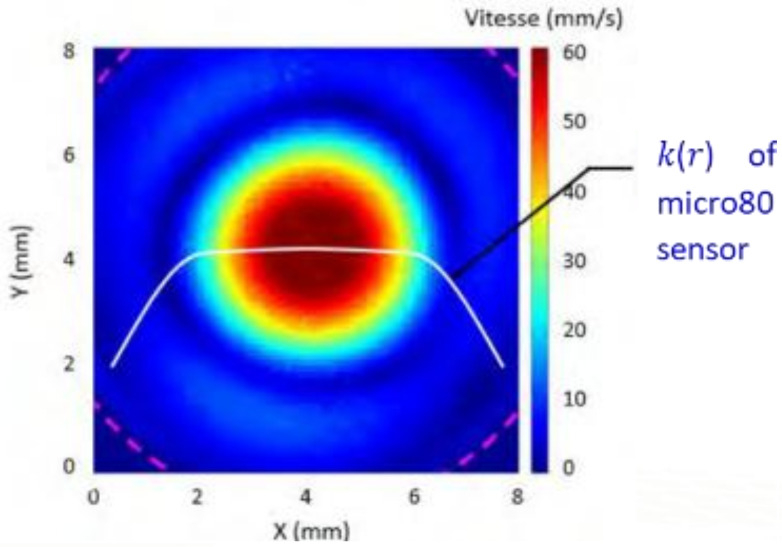

Assumption of k(r) based on weight function of various sensors[2]

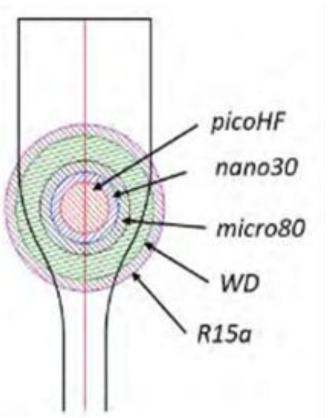

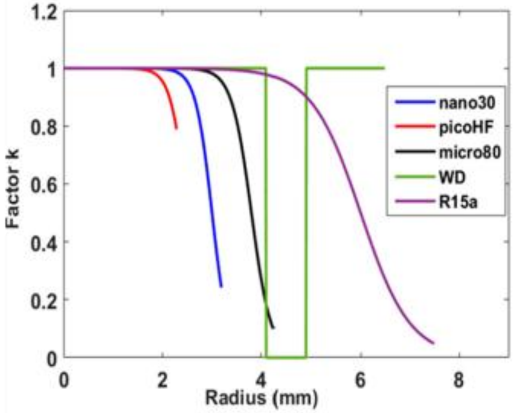

Sensor response is **non-uniform**, depending on the **sensor's geometry, spatial variations** across the sensor surface, and **operating frequency**.

The sensor response signals $v(t)$:

$$\boxed{v(t) = \frac{1}{S}\iint_S k(r).v_0(t)\,dS \quad (2)}$$

$v_0(t)$: Maximal normal velocity response;

$k(r)$: Real number from 0 to 1.

[1]. T. Monnier, S. Dia, N. Godin, and F. Zhang, "Primary calibration of acoustic emission sensors by the method of reciprocity, theoretical and experimental considerations," Journal of Acoustic Emission, vol. 30, 152–166, 2012.

[2]. N. Boulay, "Modélisation des capteurs d'émission acoustique en vue de la simulation d'un contrôle," Ph.D. thesis, Univ. Paris-Saclay, 2017.

[3]. L. Goujon and J. C. Baboux, "Behaviour of acoustic emission sensors using broadband calibration techniques," Measurement Science and Technology, vol. 14, no. 7, 903–908, 2003.

Context

Aims:

- Characterisation of the response in terms of the normal vibration velocity of AE sensors often used in wood testing : resonant sensor ($\mathrm{R}3\alpha, \mathrm{R}6\alpha, \mathrm{R}15\alpha$), and wideband sensor ($\mathrm{F}15\alpha$) (from Physical Acoustics, USA)
- Determination of the aperture function indicating the relationship between the sensitivity of AE sensor response with spatial deviation on the contact surface
- Development of the 3D models for AE wave propagation caused by the transmitting sensors by experiment and numerical simulation

Methodologies

Experimental approaches:

Measurement of the sensor's response using laser vibrometer

Table 1. *Sensor characteristics.*

Sensor models	Type of sensor	Operating frequency range
R3α	Narrowband resonance	25 kHz – 70 kHz
R6α	Narrowband resonance	35 kHz – 100 kHz
R15α	Narrowband resonance	50 kHz – 400 kHz
F15α	Wideband with a flat frequency response	100 kHz – 450 kHz

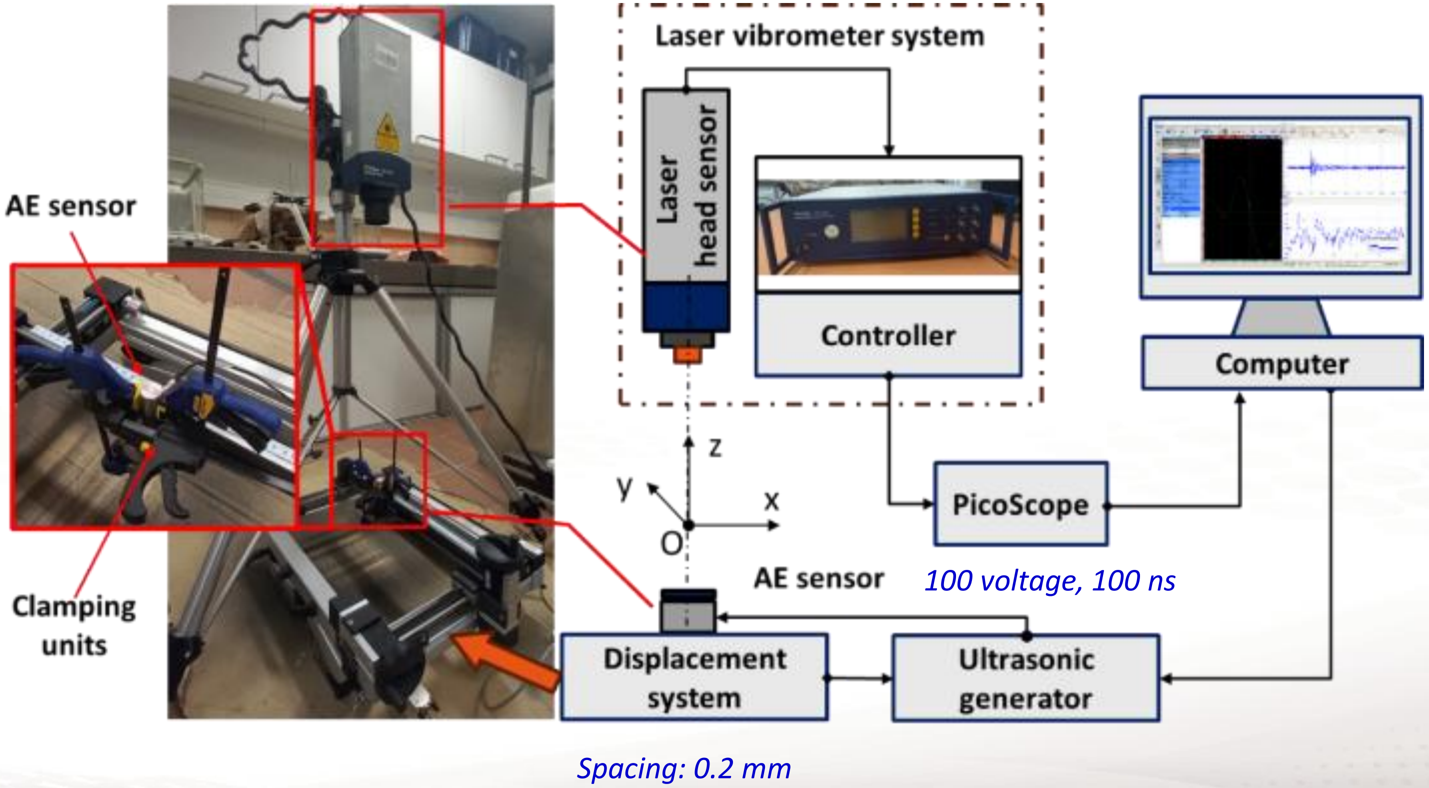

Test layout used to measure normal vibration velocity of sensor

Methodologies

Experimental approaches:

Measurement of wave propagation using the transmitting sensor in isotropic material (for reference)

Specimen:

- Aluminum, 500x500x2 (mm);
- L = 30 and 90 (mm).

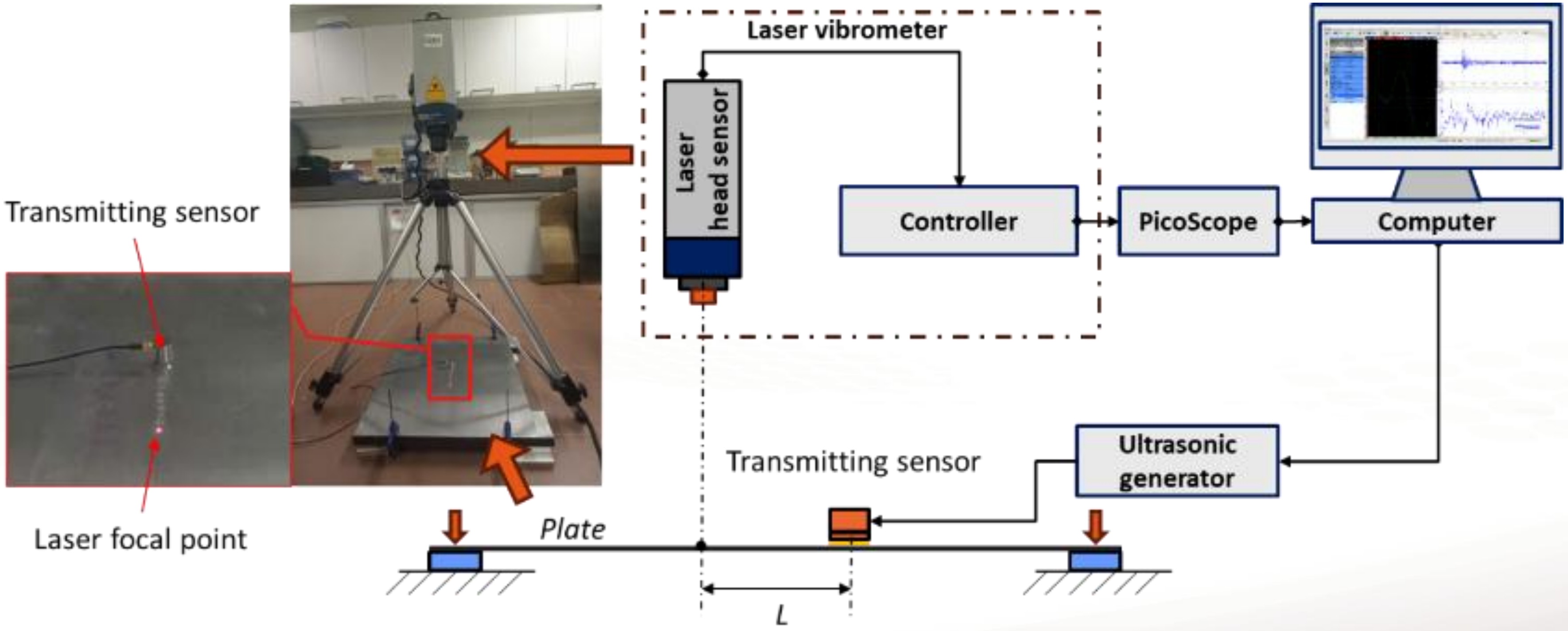

Testing setup for normal velocity measurement of AE waves generated by transmitting sensor.

Methodologies

Numerical approaches:

3D models for simulation of wave propagation used sensors' response.

3-Dimensional modelling setup

$$v(t) = \frac{1}{S}\iint_S k(r).v_0(t)\,dS \qquad (2)$$

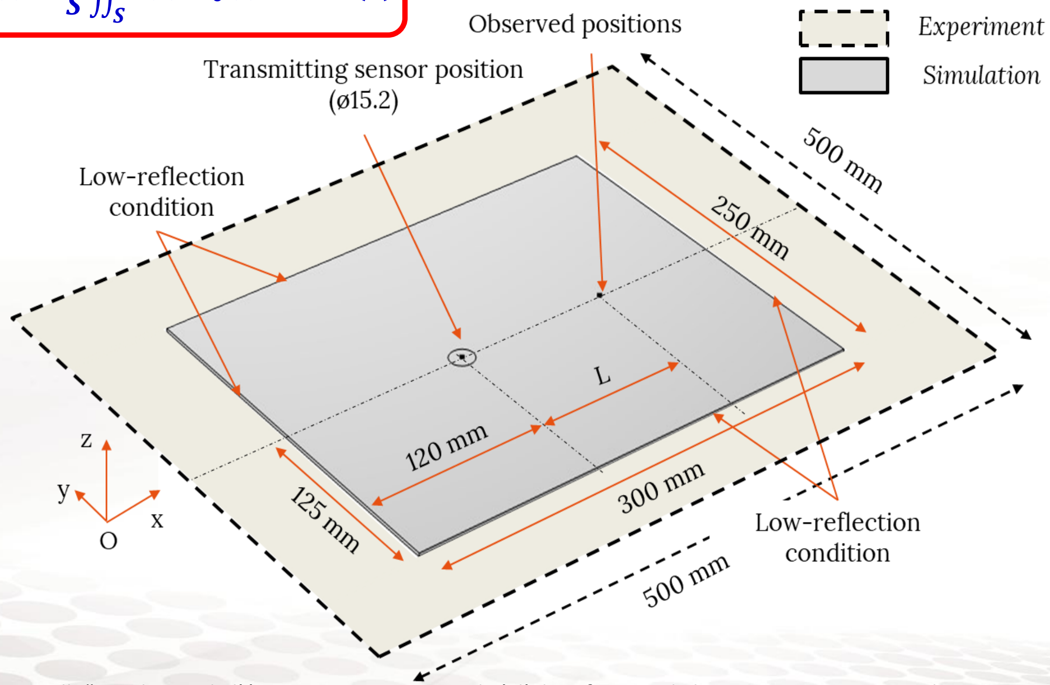

Table 2. *The information of numerical models[1].*

Density [kg/m3]	**Young's modulus** [GPa]	**Poisson's ratio**	**Longitu-dinal wave velocity** [m/s]	**Shear wave velocity** [m/s]	**Rayleigh wave velocity** [m/s]	**Damping factor** (η)	**Rayleigh damping coefficients**
2700	72	0.34	6407	3154	2944	0.002	α = 30000 β = 0

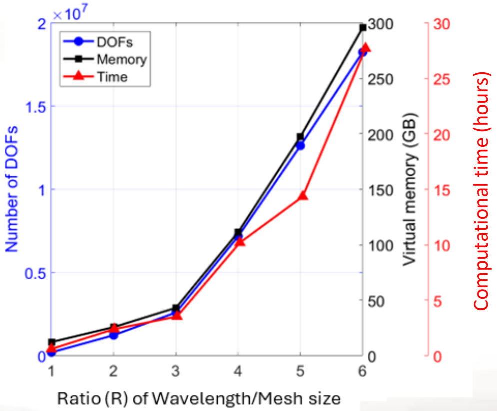

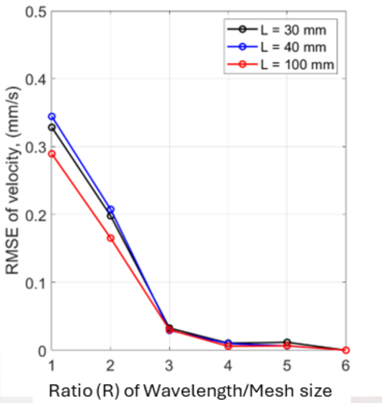

Ratio: R =3
Mesh element size: 1 mm
Time step: 0.15 µs

Mesh element convergence simulation tests

[1] T. Le Gall, "Simulation de l'émission acoustique: Aide à l'identification de la signature acoustique des mécanismes d'endommagement," Ph.D. thesis, Univ. Lyon, 2016.

Results

Sensor response in terms of normal velocity measured at the centre of the surface

R3α ***R6α*** ***R15α*** ***F15α***

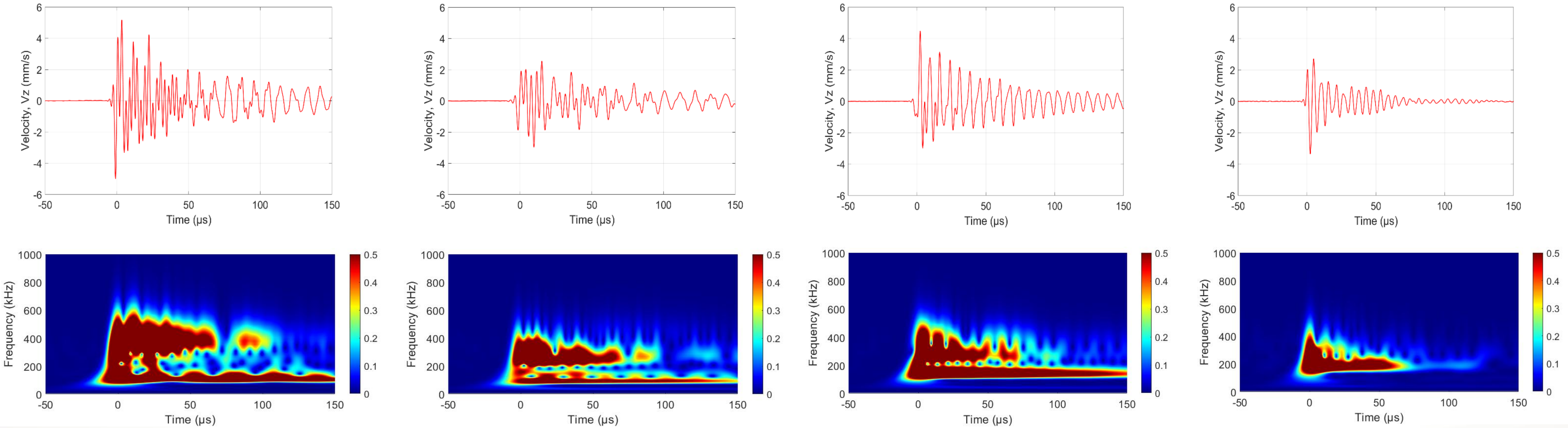

- The normal velocity response varies **depending on the type of sensors used**, peak amplitude for R3α > R15α > F15α > R6α;
- The responses of the resonant sensors ($R3\alpha$, $R6\alpha$, and $R15\alpha$) maintained **their energy at resonant frequency** longer than those of the wideband sensors with a flat frequency response (F15α);
- The **energy distribution** of the velocity response depends on the **operating frequency** characteristics and **internal structure** of sensor.

Results

Distribution of peak velocity response across whole surface and aperture effect function *k(r)*

R3α

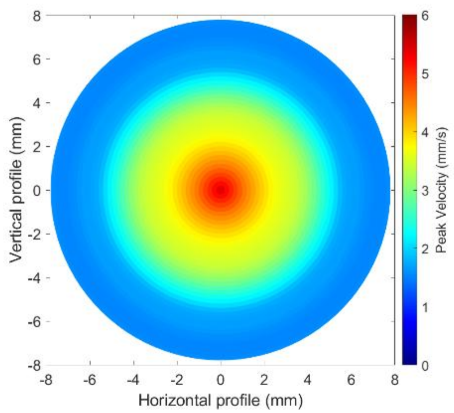

R6α

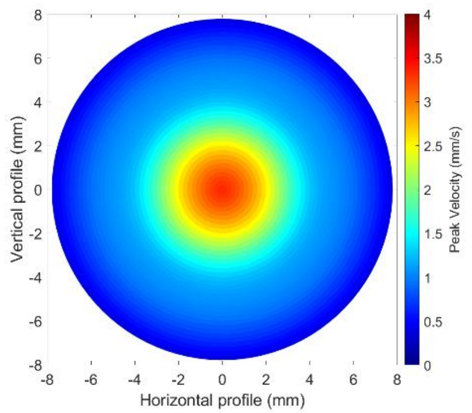

R15α

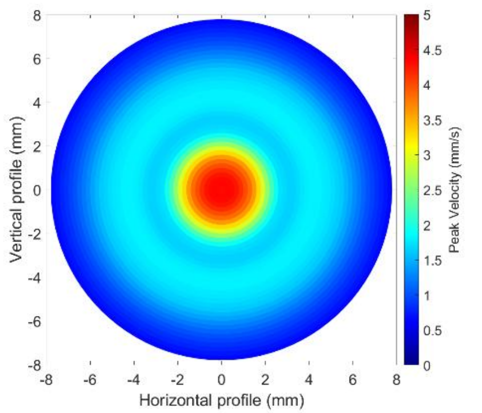

F15α

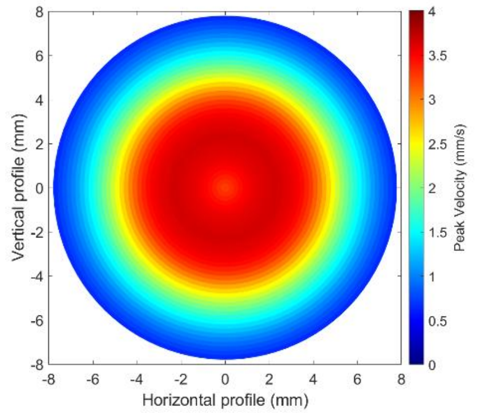

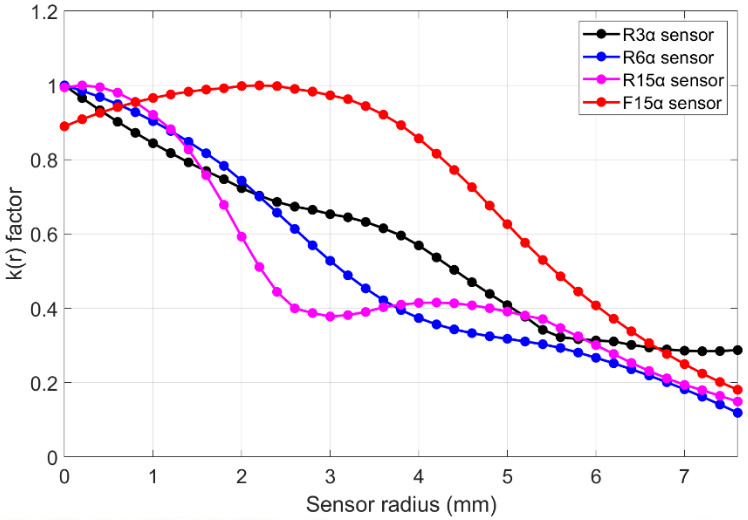

Aperture effect functions

- **Peak velocity response** significantly **depended on spatial deviations**, with the **higher values concentrated at the central area** and **decreasing towards the edges**;
- **The resonant sensors** (R3α,R6α and R15α) have **higher sensitivity responses concentrated within a small region at the centre**, whereas the **wideband sensor** (F15α) exhibited higher sensitivity distributed over a **larger surface area**;

Results

Validated results between simulations and experiments of wave velocity after propagation

R3α ***R6α*** ***R15α*** ***F15α***

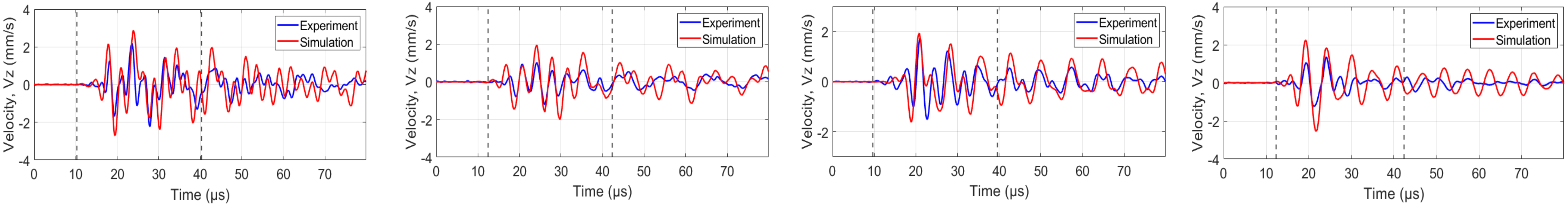

a) At transmitting sensor-to-observation point distance of 40 mm

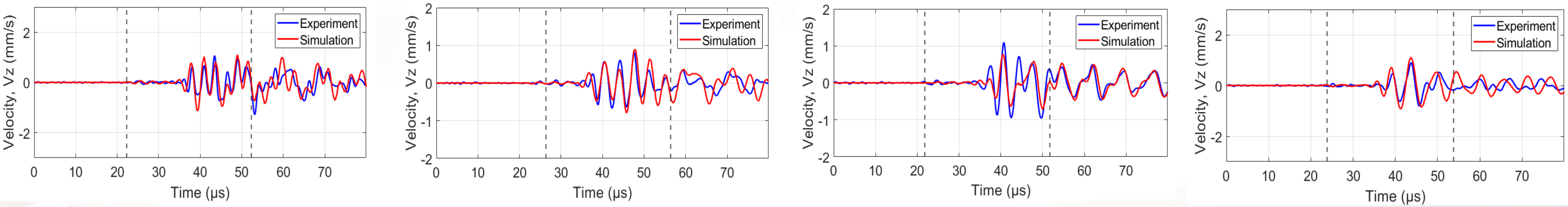

b) At transmitting sensor-to-observation point distance of 100 mm

Results

Validated results between simulations and experiments of wave velocity after propagation

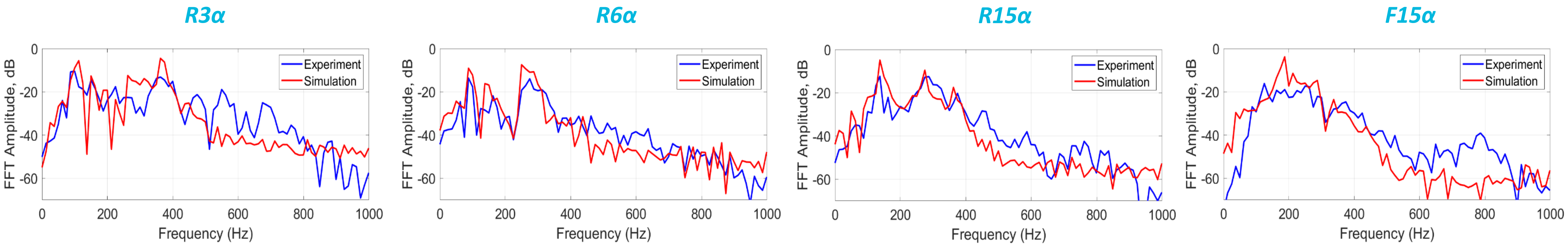

a) At transmitting sensor-to-observation point distance of 40 mm

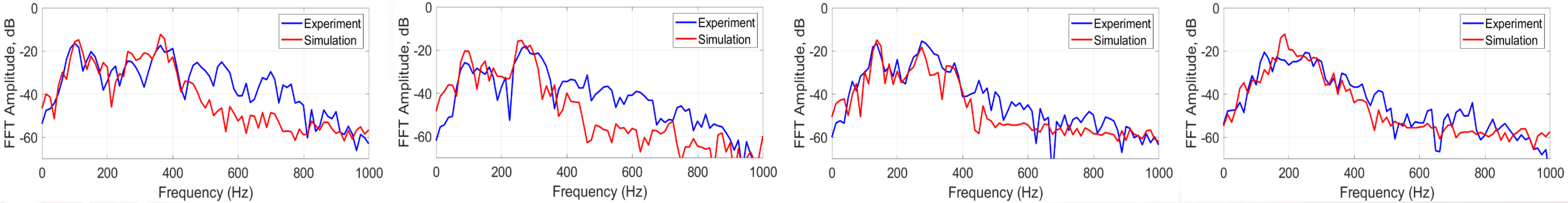

b) At transmitting sensor-to-observation point distance of 100 mm

In FFT, for vertical axis, 0 dB is referenced at 1 V/(mm/s)

INSTITUT CLÉMENT ADER

Perspectives on wood

Geometry and boundary conditions

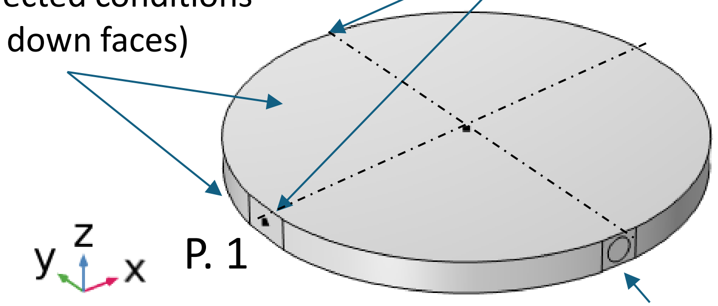

Source location ($v(t)$)

$$v_y(t) = \frac{1}{S}\iint_S k(r).v_0(t)\, dS$$

Dia. = 280 mm, thickness = 20 mm

Properties:

Type	Ash
E_T	576 MPa
E_R	900 MPa
G_{RT}	180 MPa
ν	0.68
ρ	500 Kg/m^3

Results

Time=0 µs Volume: Velocity, Y-component (mm/s)

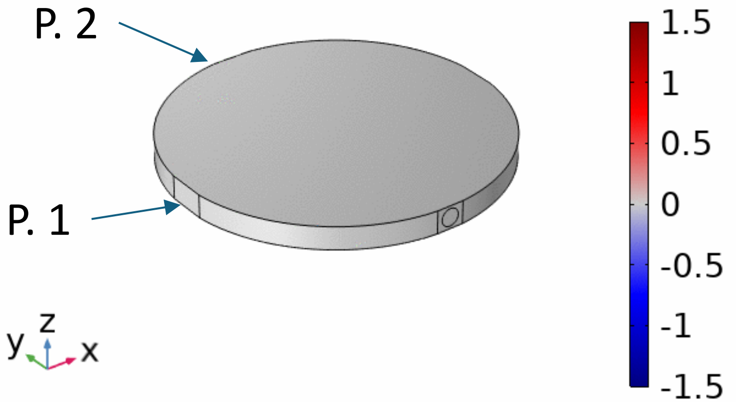

Source mechanism

$v_y(t)$

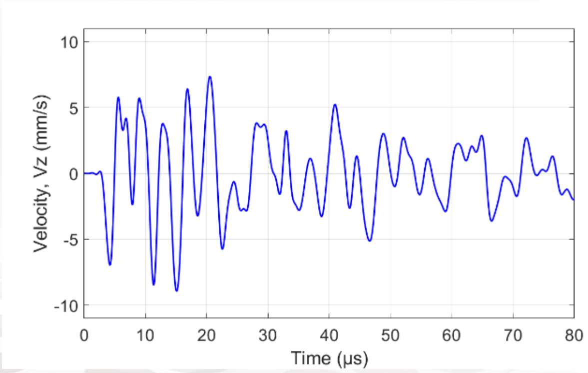

$k(r)$

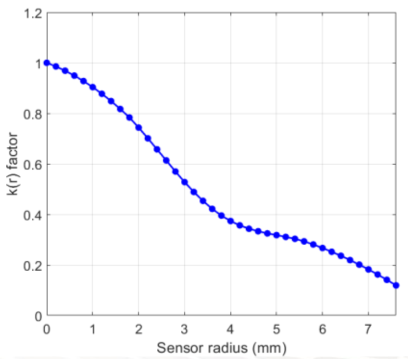

Sensor responses and aperture function of **R6α sensor**

P1 position (V_x)

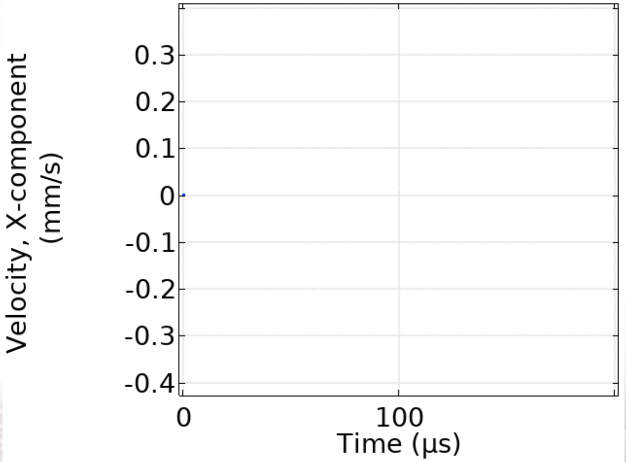

P2 position (V_y)

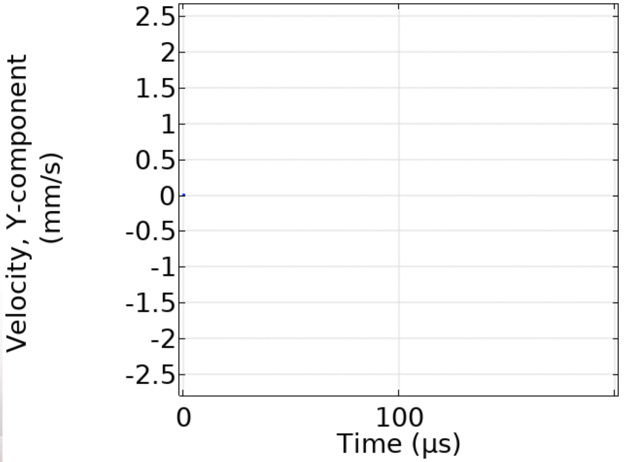

IMT Mines Albi École Mines-Télécom · INSA Toulouse · ISAE SUPAERO · Université de Toulouse · CNRS · Communauté d'universités et établissements de Toulouse

Conclusions

- **The response in term of the normal vibration velocity** of four AE sensors ($R3\alpha$, $R6\alpha$, $R15\alpha$, and $F15\alpha$) was identified
- **The aperture effect functions** of the AE sensors was explored
- **3D models for wave propagation** using sensor responses were developed by experimental and numerical simulation
- Perspectives on the use of this modelling in **wood material**